Electrochemical Preparation of VPtCl$_6$ Film and Its Electrocatalytic Properties with NAD$^+$ and Sulfur Oxoanions

Soundappan Thiagarajan,* Shen-Ming Chen,,z and Kao-Hui Lin**

Electroanalysis and Bioelectrochemistry Lab, Department of Chemical Engineering and Biotechnology, National Taipei University of Technology, Taipei 106, Taiwan

A modified electrode with vanadium hexachloroplatinate (VPtCl$_6$) film has been fabricated directly from the mixing of V^{2+} and PtCl$_6^{2-}$ ions, and its electrochemical behavior was investigated. The deposition of a VPtCl$_6$ film occurred when Pt^{IV}Cl$_6^{2-}$ was electrochemically reduced to Pt^{II}Cl$_6^{2-}$ and V^{3+} to V^{2+}. The electrochemical quartz crystal microbalance (EQCM), ultraviolet-visible absorption spectroscopy, stopped-flow, chronoamperometry, and cyclic voltammetry techniques were used to study the deposition and growth mechanism of the above film. In the EQCM studies, the reversibility of the vanadium (II/III) hexachloroplatinate film during cycling and the corresponding frequency change was found to be good, and the V^{2+} ion exchange obviously occurred in the redox couple. For the surface morphological analysis, the film was further electrochemically deposited on a transparent semiconductor indium tin oxide (ITO) electrode for scanning electron microscopy and atomic force microscopy studies. It was found that the deposited VPtCl$_6$ film formed as a film with platinum and vanadium particles on ITO. To validate the electroanalytical properties, a VPtCl$_6$-modified glassy carbon electrode was applied for the electrocatalytic reduction of the NAD$^+$ (β-Nicotinamide adenine dinucleotide) and sulfur oxoanions, and the results showed a quite effective electrocatalytic reduction for the corresponding substances.
© 2008 The Electrochemical Society. [DOI: 10.1149/1.2830846] All rights reserved.

Generally, the biochemical reactions that are catalyzed by redox enzymes such as oxidoreductases or dehydrogenases depend on the use of NAD(H) as a cofactor that plays the role of the electron and hydrogen carrier. In the reduced form, NADH, the molecule transfers two electrons and a proton to a substrate in the presence of a suitable enzyme, resulting in the oxidation of NADH to β-Nicotinamide adenine dinucleotide (NAD$^+$). In the biomedical and industrial area, the NADH has important values. The enzymatically catalyzed electroreduction of NAD$^+$ has also attracted considerable attention for both biosensor development and large-scale applications. So, the reduction of NAD$^+$ to NADH has attracted significant scientific attention over the years. Chemically modified electrodes[1-3] and enzyme-mediated electrodes[4-6] have been proposed for NAD$^+$ reduction. A number of studies have been reported, and a large majority of these relies on an electron-mediator-assisted reduction mechanism. While enzymatic modification of an electrode surface can give hopeful results in the reduction of NAD$^+$ to enzymatically active 1, 4-NADH, this method results in a somewhat complex electrode system due to problems associated with the immobilization of an enzyme and electron mediator at the electrode surface, including loss of the enzyme activity and electron mediator leakage. Hence, there is a need to develop a simple electrode surface that would allow electrochemical reduction of NAD$^+$. It is therefore desirable to design a modified electrode that would have a long-term stability and offer a high efficiency in the reduction of NAD$^+$.

The sulfur oxoanions exist in various natural ecosystems, waste waters, and in atmospheric pollutants close to industrial sites. Sulfur species with an intermediate oxidation state from −2 to +6 are produced during a variety of biotic and abiotic processes.[7-9] The presence of the sulfur compounds in biogeochemical processes plays a major role. Thus, the determination of the sulfur species has been rapidly developed over the last 10 years.[10,11] Therefore, the development of sensors sensitive to the sulfide and sulfur oxoanions is an important challenge for industrial, medical, and environmental applications. Various methods, such as titration, polarography, and colorimetry, have been reported for the determination of sulfur anions.[12,13] However, those methods are difficult to automate or suffer from numerous chemical interferences, prevented from working by solution turbidity, and demand complicated instrumentation.

Further, the iron tetrakis (N-methyl-2-pyridyl)porphyrin,[14] iron tetrakis(4-sulfonatophenyl) porphyrin,[15] poly vinyl pyridine/Pd/IrO$_2$,[16] poly NiMe4TAA (NiCTT) tetramethyl dibenzo tetraza annulenes,[17] copper hexacyano ferrate modified graphite electrode,[18] GC electrode modified with Co (II) hexacyanoferrate,[19] polynuclear mixed-valent ruthenium oxide hexacyanoruthenate film-modified electrodes,[20] and Pt electrode modified with a Prussian blue film[19,21] have been used for electrocatalytic oxidation of sulfur oxoanions and sulfide. Unfortunately, most modified electrodes come with certain disadvantages, such as considerable leaching of electron transfer mediator and poor long-term stability. Hence, it is important to investigate and develop an easy and reliable method to fabricate modified electrodes.

Further, the fundamental aspects of V(IV)/V(V) and V(II)/V(III) redox reactions and of the dissolved electroactive species are not yet completely clear. V(IV)/V(V) and V(II)/V(III) redox reactions in moderate aqueous media had been described in several reports.[22-24] Electrochemically active film-modified electrodes show interesting features in redox chemistry that is accompanied by changes in their ion exchange and electrocatalytic properties. The uses of metal hexachloroplatinates, similar to metal hexacyanoferrate film-modified electrodes for cation (or anion) sensors,[25-29] are of interest for practical applications. For example, in the field of chemistry and materials science there is the electropolymerized metal complex of iron hexacyanoferrate films, which exhibits a high selectivity for ion exchange, and exhibits cation exchange reactions with Li$^+$, Na$^+$, K$^+$, Rb$^+$, and Cs$^+$. The electron transfer reactions of copper hexabromoplatinate films show that redox processes occur when Cu^{2+} ions are present in the aqueous solution and when they are immobilized in a hexabromoplatinate film on an electrode's surface.[30,31] These redox processes occur via a diffusionless film electron transfer process in the case of the redox reaction of copper (II/I) hexabromoplatinate films, and by Cu^{2+} ion diffusion between the film and aqueous solution in the case of aqueous Cu^{2+} ions.

The fabrication of a chemically modified film electrode is easily controlled by repeated cyclic voltammetry as the synthetic procedure, with an increase in the peak current of a modified film indicating an appropriate redox couple for the film. Simultaneous cyclic voltammetry and microgravimetry, using an electrochemical quartz crystal microbalance (EQCM), UV-visible absorption spectroscopy, stopped-flow kinetic method, and chronoamperometric experiments, can detect the surface reactions on an electrode in an experimental solution, and so they are useful methods for monitoring the deposition and the growth of metal hexachloroplatinate films, as the syn-

* Electrochemical Society Student Member.
** Electrochemical Society Active Member.
z E-mail: smchen78@ms15.hinet.net

thesis of a metal hexachloroplatinate film requires an electrochemical reaction. Electrocatalytic activity measurements can provide information on analytical applications, and on the electrochemical transfer activity for the relatively electroactive compounds. Practical applications of metal hexabromoplatinate film-modified electrodes are used as electrochemical sensors for determining the concentrations of dopamine, NAD$^+$, NADH, and sulfur oxoanions.[31] Here, we report on the preparation of an electrochemically active and stable vanadium hexachloroplatinate (VPtCl$_6$) film directly synthesized from the mixing of V^{2+} and PtCl$_6^{2-}$ ions in an aqueous KCl pH 3.0 solutions. The EQCM, cyclic voltammetry, chronoamperometry, and UV-visible absorption spectroscopy were used to study the interaction of V^{2+} and PtCl$_6^{2-}$ ions and the in situ growth of the vanadium hexachloroplatinate films, along with studying their electrochemical properties and V^{2+} ion exchange properties. The results showed that the deposition of a vanadium hexachloroplatinate film occurred when Pt^{IV}Cl$_6^{2-}$ was electrochemically reduced to Pt^{II}Cl$_6^{4-}$ and V^{3+} to V^{2+}. To evaluate the practical analytical utility, the VPtCl$_6$ film-modified glassy carbon electrode (GCE) was used as an electrochemical sensor for the electrocatalytic reduction of NAD$^+$ and sulfur oxoanions.

Experimental

Reagents.— The NAD$^+$ was purchased from Sigma-Aldrich, USA. The other reagnts were of analytical grade. All solutions were prepared with double-distilled water. All the experimental results were obtained at room temperature. The 0.1 M aqueous KCl solution at pH 3.0 was used for the film preparation and the other electrocatalytic experiments.

Apparatus.— The electrochemistry was performed using a Bioanalytical Systems model CV-50W and CH Instruments model CHI-400 and CHI-750 potentiostats. A conventional three-electrode system was used throughout the experiments. The BAS GCEs were in the form of disks ($\varphi = 0.3$ cm in diameter) sealed in a Teflon jacket having an exposed geometric surface area of 0.07 cm^2. The working electrode was bare or VPtCl$_6$ film-modified GCE, the auxiliary electrode was a platinum wire, and a Ag/AgCl electrode was used as a reference. All the potentials mentioned in this paper were referred to this reference electrode. The working electrode for the EQCM measurements was an 8 MHz AT-cut quartz crystal with gold electrodes. The diameter of the quartz crystal was 13.7 mm and the gold electrode diameter was 5 mm. All the EQCM measurements were carried out at room temperature. For the scanning electron microscopy (SEM) and atomic force microscopy (AFM) analyses, an indium tin dioxide (ITO) electrode (which was composed of ITO that was sputtered on a glass substrate) was used. The morphological characterizations of the films were examined by means of SEM (Hitachi S-3000H) and AFM (Being Nano-Instruments CSPM-4000). UV-visible absorption spectra were measured using a Hitachi model U-3300 spectrophotometer. Kinetic measurements were performed using a Bio-Logic stopped-flow module SFM-20, which consisted of a mechanical subsystem and a power supply. The fast reaction spectrometer was an optical system composed of an MOS-250 spectrophotometer and spectrofluorometer. The amperometric experiment was performed with a Pine Instrument Co. electrode in conjunction with a CH Instruments CHI-750 potentiostat connected to a model AFMSRX analytical rotator.

Film preparation.— Prior to electrodeposition of the VPtCl$_6$ film, the GCE was polished with the help of a BAS polishing kit with aqueous slurries of successively finer alumina powder (0.05 μm), rinsed, and ultrasonicated in double-distilled deionized water. The electrochemical formation of vanadium hexachloroplatinate (VPtCl$_6$) films was performed by continuous cycling of the potential of the working electrode in a defined potential range using a suitable scan rate in a 0.1 M aqueous KCl solution at pH 3.0, containing V^{2+} (or V^{3+}) and PtCl$_6^{2-}$.
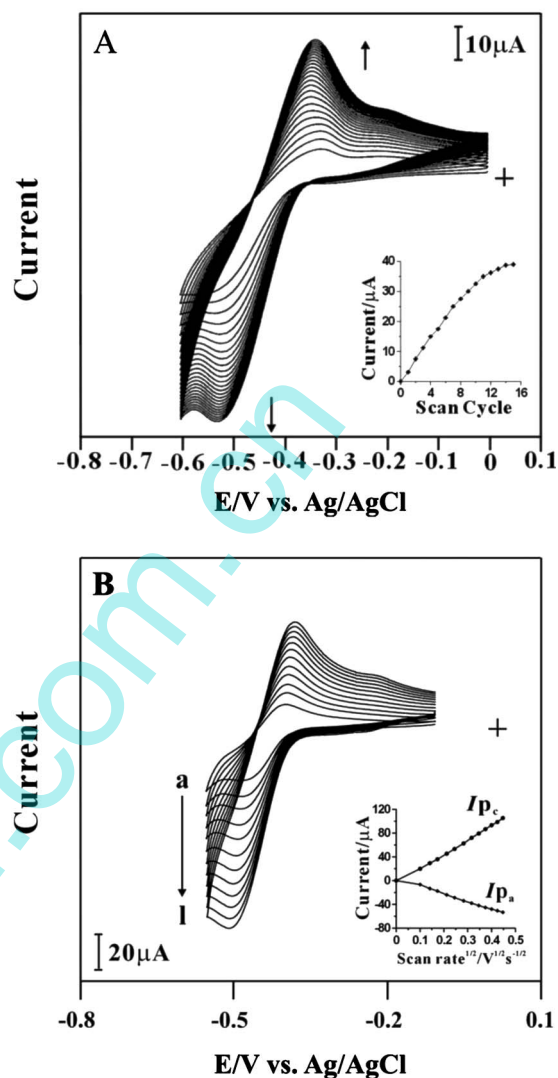

Figure 1. (A) Cyclic voltammograms of a GCE modified with a VPtCl$_6$ film synthesized from 3×10^{-3} M V^{2+} and 2×10^{-4} M PtCl$_6^{2-}$ in a 0.1 M aqueous KCl solution at pH 3.0. Switching potential between 0 and -0.6 V. The inset shows a plot of the anodic peak current vs scan cycle. (B) Cyclic voltammogram of VPtCl$_6$ film in a 0.1 M aqueous KCl solution (pH 3.0) and scan rate (a) 0.01, (b) 0.02, (c) 0.03, (d) 0.045, (e) 0.06, (f) 0.08, (g) 0.10, (h) 0.12, (i) 0.14, (j) 0.16, (k) 0.18, (l) 0.20 V s^{-1}. The inset shows a plot of the peak currents Ip_c and Ip_a vs (scan rate)$^{1/2}$.

Results and Discussion

Electrochemical growth of the VPtCl$_6$ film.— Figure 1A shows the repetitive cyclic voltammograms of a VPtCl$_6$ film electrodeposited from 3×10^{-3} M V^{2+} and 2×10^{-4} M PtCl$_6^{2-}$ in a 0.1 M aqueous KCl solution at pH 3.0 in the scanning potential region between 0.0 and -0.6 V on a GCE. In the first cycle, the reduction and oxidation peaks of V^{3+} and V^{2+} appeared in the forward and reverse segments, respectively. Upon continuous cycling, the peak currents corresponding to the redox couple were found to be increased. This activity confirms the deposition of VPtCl$_6$ film on the electrode surface. Further, the obtained result shows that the cyclic voltammogram of the VPtCl$_6$ film exhibited one redox couple with formal potentials of -0.43 V (vs Ag/AgCl). This single redox couple was attributed to the $[V_2^{II}Pt^{II}Cl_4Pt^{IV}Cl_6]/[V_3^{II}Pt^{II}Cl_4Pt^{II}Cl_6]$ redox reaction.[22-24,30,31] The inset of Fig. 1A shows the VPtCl$_6$ film growth process (anodic peak current vs the scan cycle).

Electrochemical properties of the VPtCl$_6$ film.— Further, the deposited film was transferred to 5×10^{-3} M V^{2+} in a 0.1 M aqueous KCl pH 3.0 solution for the different scan rate studies. Figure 1B shows the electrochemical behavior of the VPtCl$_6$ film in a 0.1 M aqueous KCl pH 3.0 solution for different scan rate studies. Here, the anodic and cathodic peak currents of the film were increased linearly with the scan rate. Further, the inset of Fig. 1B shows that the plot of Ip_c and Ip_a vs (scan rate)$^{1/2}$ showed a linear dependence of the anodic and cathodic peak currents with the scan rate. Here, the peak current and the scan rate are also related as

$$Ip = kn^{3/2}AD_oC_o\nu^{1/2} \qquad [1]$$

where k, n, A, D_o, C_o, and ν represent a constant, the electron transfer number, the area of the working electrode, a diffusion coefficient, the concentration of the reactant, and the scan rate, respectively. If this behavior were to be consistent with a diffusionless and reversible electron transfer process at low scan rates, then the peak current and scan rate would be related as[32,33]

$$Ip = n^2F^2\nu A\Gamma_o/4RT \qquad [2]$$

Γ_o, ν, A, and Ip represents the surface coverage concentration, the scan rate, the electrode area, and the peak current, respectively. However, both Ip_a and Ip_c have a close linear dependence on the square root of the scan rate, illustrating the reversible electron transfer process between the film and aqueous solution. Finally, from the above results it is concluded that the redox process was confined to the forward and backward reversible process, and the redox couple immobilized VPtCl$_6$ film was involved with the presence of vanadium ion exchange in the solution.

Next, the Pt^{IV}Cl$_6^{2-}$ to Pt^{II}Cl$_6^{4-}$ reduction and the oxidation of Pt^{II}Cl$_6^{4-}$ to Pt^{IV}Cl$_6^{2-}$ are shown in Fig. 2A. Figure 2A shows that the first segment scan (positive scan) began at an initial potential of +0.4 V, and the positive scan was carried out to a potential of 1.2 V (Fig. 2A, segment 1). In the second segment, it was initiated at 1.2 V; the negative scan at potentials between 1.2 and −0.55 V is shown in Fig. 2A (segment 2). Also, the third segment was an initiated potential at −0.55 V and a positive scan between potentials of −0.55 and 1.2 V (Fig. 2A, segment 3). Here, the reduction peak current that arose from the conversion of Pt^{IV}Cl$_6^{2-}$ to Pt^{II}Cl$_6^{4-}$ was observed with a cathodic peak potential at about −0.32 V, and the oxidation peak current that arose from the conversion of Pt^{II}Cl$_6^{2-}$ to Pt^{IV}Cl$_6^{4-}$ was observed with an anodic peak potential at about +0.95 V. Furthermore, Fig. 2B shows that the value of the cathodic current for the reduction of V^{3+} to V^{2+} exhibits an unobvious behavior in pH 3.0 than in an acidic aqueous solution. In Fig. 2C, the cyclic voltammogram shows that V^{3+}/V^{2+} and V(IV)/V(V) redox couples[23] exhibited a formal potential at about −0.45 and +1.13 V (vs Ag/AgCl) in 12 M H$_2$SO$_4$ solution. The reversible values for the V^{2+}/V^{3+}, V^{3+}/VO^{2+}, and VO^{2+}/VO$_2^+$ couples are established[22,24] at various electrode materials. Thus, the redox couple at −0.45 V is related to the V^{3+}/V^{2+} redox couple, the redox couple at +1.13 V is related to the VO^{2+}/VO$_2^+$ redox couple, and the redox couple at +0.85 V is related to the V^{3+}/VO^{2+} redox couple as shown in Fig. 2C. Further, Table I could explicate the electrochemical properties of the VPtCl$_6$ film in various acidic aqueous solutions.

VPtCl$_6$ film deposition using EQCM technique.— The EQCM measurement was used as a good method for monitoring the in situ growth of vanadium hexachloroplatinate on gold electrodes. Figure 3 shows the change in the EQCM frequency resulting from the growth of the VPtCl$_6$ film on the gold electrode. The successful growth of VPtCl$_6$ film (Fig. 3A) obtained from 1×10^{-3} M V^{2+} and 1×10^{-4} M PtCl$_6^{2-}$ in a 0.1 M aqueous KCl pH 3.0 solution showed a single redox couple between the potentials of 0.0 and −0.6 V. Figure 3B shows the change in the EQCM frequency recorded during the first 16 segments of the repeated cyclic voltammograms. Here, the voltammetric peak current in Fig. 3A and the frequency decrease (or mass increase) in Fig. 3B remained consis-
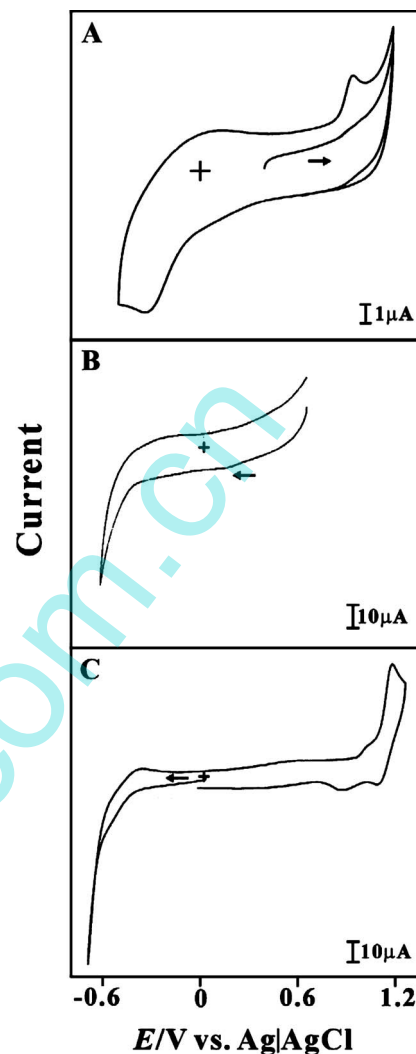

Figure 2. (A) 2×10^{-4} M PtCl$_6^{2-}$, (B) 1×10^{-3} M V^{2+} in a 0.1 M aqueous KCl solution at pH 3.0, (C) 8×10^{-3} M V^{2+} in a 12 M H$_2$SO$_4$ solution. Scan rate = 0.1 V s^{-1}.

tent with the growth of a VPtCl$_6$ film on the gold electrode. The EQCM results showed that the deposition of the film occurred obviously within the potential range of −0.25 to −0.6 V (vs Ag/AgCl). From the change in mass at the quartz crystal in the EQCM, the VPtCl$_6$ film growth process exhibited obvious changes in the frequency in the potential range between 0 and −0.6 V, while Pt^{IV}Cl$_6^{2-}$ was reduced to Pt^{II}Cl$_6^{2-}$ in the 0.1 M aqueous KCl pH 3.0 solution. The deposition processes initially involved oxidation of the V^{2+} species by Pt^{IV}Cl$_6^{2-}$ changed into Pt^{II}Cl$_6^{2-}$; then, V^{3+} can be reduced into V^{2+} electrochemically in an aqueous solution. This V^{2+} reacts with Pt^{II}Cl$_4^{4-}$ and Pt^{IV}Cl$_6^{2-}$ to form VPtCl$_6$ film on the electrode surface. The EQCM results show that the VPtCl$_6$ film growth process was slower as, being a chemical reaction, Pt^{IV}Cl$_6^{2-}$ was reduced to Pt^{II}Cl$_4^{2-}$ (Fig. 3B). The relatively large mass of VPtCl$_6$ film deposition occurred during the second and third scan cycle. The comparison of the first scan cycle was reflected in the increased frequency change from the film adhering to the gold electrode surface. The rate of film growth (from the change in frequency) during the second and third scan cycle was found faster than the first scan cycle (Fig. 3B) on the (initially) clean gold electrode surface. Further, the change in mass at the quartz crystal was calculated from the change in the observed frequency using the Sauerbrey equation[34,35]

Table I. Electrochemical properties of the VPtCl$_6$ film formation in acidic aqueous solutions.

Film or component	Formal or peak potential (V)	Assignment	Acidity
VPtCl$_6$ film	−0.43	Formal potential	pH 3.0
V(II)/V(III) redox couple	−0.45	Formal potential	12 M H$_2$SO$_4$
V(IV)/V(V) redox couple	+1.13	Formal potential	12 M H$_2$SO$_4$
Pt^{IV}Cl$_6^{2-}$	−0.32	Cathodic peak potential	pH 3.0
Pt^{II}Cl$_6^{4-}$	+0.95	Anodic peak potential	pH 3.0

$$\text{Mass change}(\Delta m) = (-1/2)(f_o^{-2})(\Delta f)A(k\rho)^{1/2} \qquad [3]$$

where A is the area of the gold disk coated onto the quartz crystal, ρ is the density of the crystal, k is the shear modulus of the crystal, Δf is the measured frequency change, and f_o is the oscillation frequency of the crystal. A frequency change of 1 Hz is equivalent to a 1.4 ng change in mass. During the first cycle scan, about 86 ng/cm^2 of a VPtCl$_6$ film was deposited on the fresh gold electrode, and a total of about 1036 ng/cm^2 of a VPtCl$_6$ film was deposited on the gold electrode after the first eight cyclic voltammetric scans.

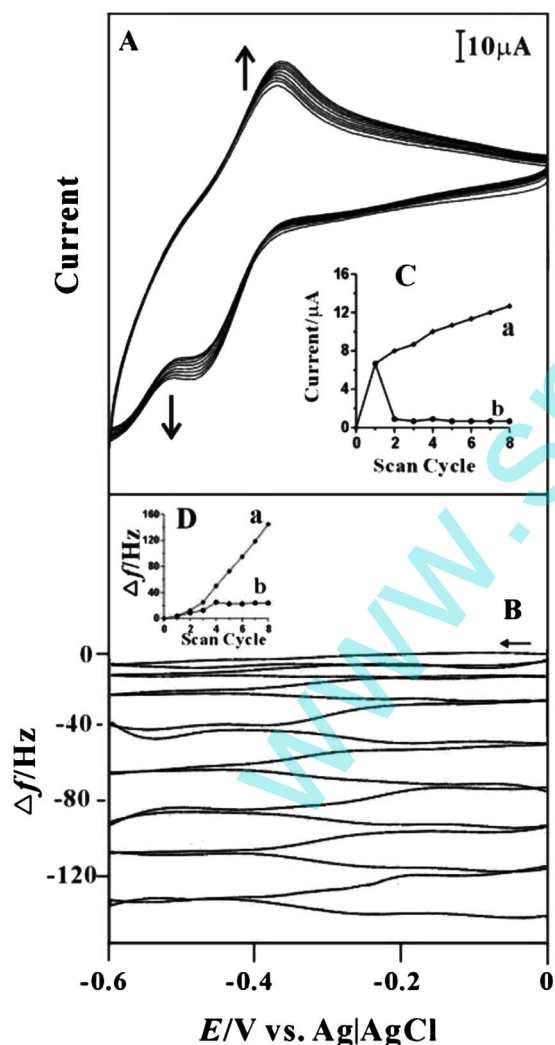*The ion exchange and electrochemical properties of VPtCl$_6$ film in EQCM.*— Figure 4A and 4B shows the change in the EQCM

Figure 3. (A) Cyclic voltammograms of a gold electrode modified with a VPtCl$_6$ film synthesized from 1×10^{-3} M V^{2+} and 1×10^{-4} M PtCl$_6^{2-}$ in a 0.1 M aqueous KCl solution at pH 3.0. Electrode = gold. Scan rate = 0.02 V s^{-1}. (B) The change in EQCM frequency recorded concurrently with the consecutive cyclic voltammograms of (A); (C) (a) plot of the anodic peak current vs scan cycle. (b) Every cycle of the anodic peak current change vs scan cycle; (D) (a) the total frequency change Δf vs the scan cycle and (b) every cycle frequency change Δf vs the scan cycle.
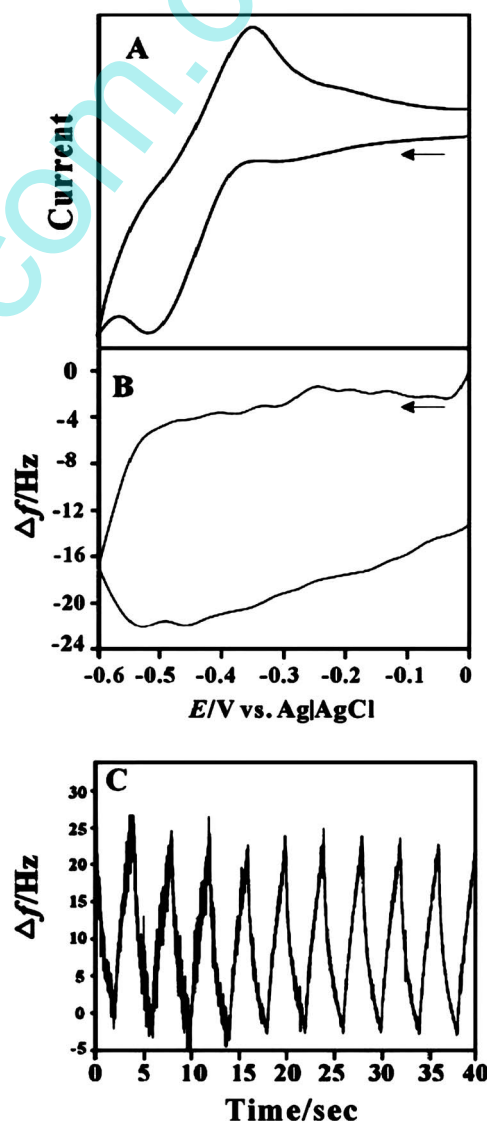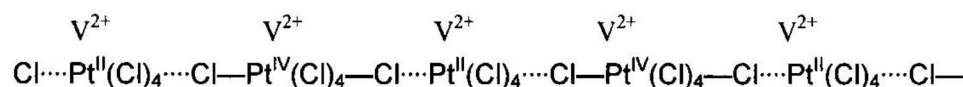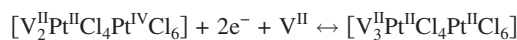

Figure 4. (A) Cyclic voltammogram of a gold disk electrode modified with VPtCl$_6$ film for 1×10^{-3} M V^{2+} in a 0.1 M aqueous KCl pH 3.0 solution and (B) the microgravimetric cyclic voltammetric response of a VPtCl$_6$ film on a gold disk electrode for 1×10^{-3} M V^{2+} in 0.1 M aqueous KCl pH 3.0 solution. Scan rate = 0.02 V s^{-1}. (C) EQCM measurements of VPtCl$_6$ film on a gold disk electrode for 1×10^{-3} M V^{2+} in a 0.1 M aqueous KCl pH 3.0 solution during potential switching from $E_{appl} = -0.2$ to -0.8 V (vs Ag/AgCl) using a time pulse of 2 s.

$$V^{2+} \qquad V^{2+} \qquad V^{2+} \qquad V^{2+} \qquad V^{2+}$$

$$Cl\cdots Pt^{II}(Cl)_4\cdots Cl-Pt^{IV}(Cl)_4-Cl\cdots Pt^{II}(Cl)_4\cdots Cl-Pt^{IV}(Cl)_4-Cl\cdots Pt^{II}(Cl)_4\cdots Cl-$$

Scheme 1. The expected structure for the VPtCl$_6$ film.

frequency recorded during the cyclic voltammetry in the presence of V^{2+} and VPtCl$_6$ film in pH 3.0 aqueous solutions. The results showed that the frequency decrease (i.e., mass increase) in Fig. 4B is consistent with the mass change that occurred between the potentials from 0.0 to -0.6 V (vs Ag/AgCl). Here, the change in frequency (mass) between the potentials of 0.0 and -0.6 V (i.e., the redox couple region of the vanadium hexachloroplatinate) was found to be obvious (Fig. 4B). This behavior is due to the V^{2+} exchange during the reduction Pt (VI) present in the platinum hexachloroplatinate to Pt (II) in the potential range 0.0 to -0.6 V. From the kinetics of EQCM and chronocoulometry measurements (Fig. 4A-4C), the potential switching from 0.0 to -0.6 V of a VPtCl$_6$ film in an aqueous KCl pH 3.0 solution was determined. In these experiments, a square wave potential was applied over a period of 2 s during the film cation exchange, as shown in Fig. 4C. Here, the reversibility of the VPtCl$_6$ film during cycling was consistent with the changing frequency and charge, and confirmed the V^{2+} ion exchange occurrence with the redox couples. A decrease in the frequency (or increase in the mass) was proposed during the reduction of film in the potential range of 0.0 and -0.6 V

$$[V_2^{II}Pt^{II}Cl_4Pt^{IV}Cl_6] + 2e^- + V^{II} \leftrightarrow [V_3^{II}Pt^{II}Cl_4Pt^{II}Cl_6]$$

Finally, the proposed structure of the film (reduced form) is shown in Scheme 1.[32,33]

The UV absorption spectra shown in Fig. 5A also reveal a reaction between Pt^{IV}Cl$_6^{2-}$ and V^{2+}. Here, the reduction peak of Pt^{IV}Cl$_6^{2-}$ to Pt^{II}Cl$_6^{4-}$ is not obvious when V^{2+} is added to the aqueous solution (Fig. 5A). During the electrochemical process, the spectral change
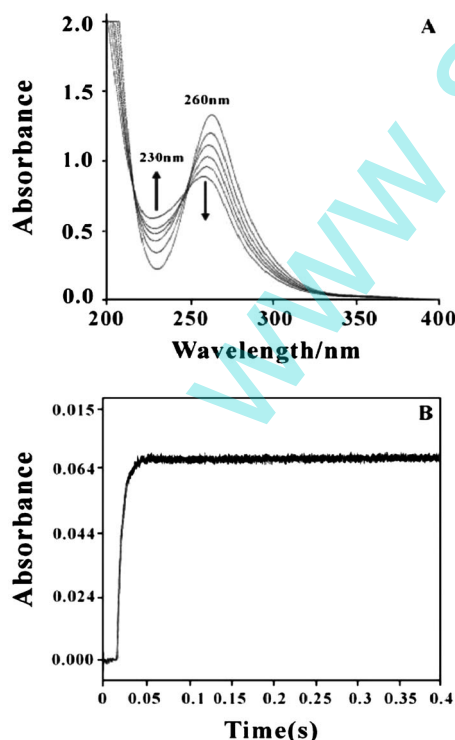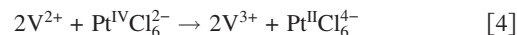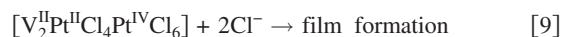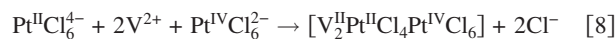

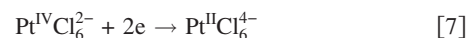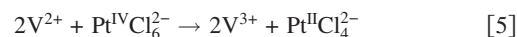**Figure 5.** (A) UV-visible absorption spectra of V^{2+} gradually added (2 × 10^{-6} M divided in seven aliquots) to 1 × 10^{-4} M PtCl$_6^{2-}$ at pH 3.0 aqueous solutions. (B) Stopped-flow kinetic measurements at a wavelength of 230 nm for 1 × 10^{-4} M V^{2+} in a 0.1 M aqueous KCl pH 3.0 solution mixed with PtCl$_6^{2-}$ with 1 × 10^{-4} M. $k = 51.03$ s and $t_{1/2} = 0.013$.

on reaction of Pt^{IV}Cl$_6^{2-}$ with V^{2+} showed that Pt^{IV}Cl$_6^{2-}$ was reduced to Pt^{II}Cl$_6^{4-}$ and that V^{2+} was oxidized to V^{3+} in a pH 3.0 aqueous solution. The absorption intensity $\lambda_{max} = 260$ nm decreased, and the absorption change at $\lambda = 230$ nm increased when the isosbestic point of Pt^{IV}Cl$_6^{2-}$ was reduced by the V^{2+}. The expected reaction mechanism is given below[36,37]

$$2V^{2+} + Pt^{IV}Cl_6^{2-} \rightarrow 2V^{3+} + Pt^{II}Cl_6^{4-} \qquad [4]$$

Furthermore, the stopped-flow kinetic measurements (STF) at $\lambda = 350$ and 260 nm of 1 × 10^{-3} M V^{2+} in a pH 3.0 aqueous solution mixed with a K$_2$PtCl$_6$ concentration of 1 × 10^{-4} M were examined (Fig. 5B). The change in the absorbance of the stopped-flow kinetic measurements at a wavelength of 230 nm is shown in Fig. 5B. From this result, we can conclude that the Pt^{IV}Cl$_6^{2-}$ was reduced by the V^{2+} rapidly to yield a Pt^{II}Cl$_6^{4-}$ species with a half life ($t_{1/2}$) of approximately 0.013 s. Finally, we calculated the rate constant (κ) as 51.0 s^{-1} from the data of Pt^{IV}Cl$_6^{2-}$ concentrations of 1 × 10^{-4}, 5 × 10^{-5}, and 2.5 × 10^{-5} M and a V^{2+} concentration of 1 × 10^{-3} M. Based on the results of EQCM, UV-visible absorption spectroscopy, cyclic voltammetry, and stopped-flow kinetic measurement, the mechanism for the VPtCl$_6$ film growth was interpreted. Here, the chemical reaction where Pt^{IV}Cl$_6^{2-}$ was reduced to Pt^{II}Cl$_6^{4-}$ by V^{2+} is the initiation step; then, the formed V^{3+} was reduced to V^{2+} electrochemically, and then V^{2+} reacted with the Pt^{II}Cl$_6^{2-}$, which was also formed by an electrochemical reduction and Pt^{IV}Cl$_6^{2-}$ to yield VPtCl$_6$ film. In particular, the one-dimensional chains on the electrode surface consisted of square planar d^8 Pt^{2+} complexes and octahedral d^6 Pt^{4+} complexes in the alternative method. Thus, the electrochemically deposited film was made up of mixed-valent platinum complexes loaded along in one dimension. We have elected to use VPtCl$_6$ to denote the film because here V^{2+} and PtCl$_6^{2-}$ ions are essential ions for the film formation. Thus, the reaction process in aqueous KCl pH 3.0 solutions is proposed as follows[38]

$$2V^{2+} + Pt^{IV}Cl_6^{2-} \rightarrow 2V^{3+} + Pt^{II}Cl_4^{2-} \qquad [5]$$

$$V^{3+} + e^- = V^{2+} \qquad [6]$$

$$Pt^{IV}Cl_6^{2-} + 2e \rightarrow Pt^{II}Cl_6^{4-} \qquad [7]$$

$$Pt^{II}Cl_6^{4-} + 2V^{2+} + Pt^{IV}Cl_6^{2-} \rightarrow [V_2^{II}Pt^{II}Cl_4Pt^{IV}Cl_6] + 2Cl^- \qquad [8]$$

$$[V_2^{II}Pt^{II}Cl_4Pt^{IV}Cl_6] + 2Cl^- \rightarrow \text{film formation} \qquad [9]$$

Furthermore, Fig. 6A shows the cyclic voltammogram of the VPtCl$_6$ film in the absence of V^{2+} (Fig. 6A, part a), and in the presence of V^{2+} (Fig. 6A, parts b–d) in the acidic (pH 3.0) aqueous solution. In the absence of V^{2+}, the cyclic voltammogram of the VPtCl$_6$ film showed no obvious redox couples (Fig. 6A, part a). In the presence of V^{2+}, the peak current of the redox couple of the VPtCl$_6$ film increased with increasing concentration of V^{2+}. A new redox couple of VPtCl$_6$ film appeared at about -0.43 V (Fig. 6A, part b–d). Furthermore, the typical amperometric *I-T* experiment using a VPtCl$_6$ film-modified electrode in various concentrations of V^{2+}, was performed in a well-stirred solution (rotation speed = 1200 rpm) by keeping the disk electrode potential at -0.8 V in pH 3 aqueous solution (Fig. 6B). In the amperometric experiment, a good response was obtained for the 15 sequential additions of each 5 × 10^{-5} M V^{2+} on the VPtCl$_6$ film/GC-modified disk electrode (Fig. 6B, part a) and bare glassy carbon ring electrode (background, Fig. 6B, part b). From the above results, it was observed that the reduction current of VPtCl$_6$ film, increased with the addition of V^{2+}, reached the steady

Figure 7. SEM images of ITO electrode modified with a VPtCl$_6$ film.

was characterized by using the AFM technique for the more detailed studies. AFM images provide comprehensive information about the surface morphology regarding the formation of VPtCl$_6$ film. The film was characterized by employing AFM in the tapping mode. Here, a clear interpretation of the morphology of the VPtCl$_6$ film was obtained. The AFM parameters were evaluated for a 10,000 × 10,000 nm surface area. Figure 8A depicts the tapping mode image of the VPtCl$_6$ film. Figure 8B and 8C shows the amplitude and phase of the same image. Figure 8D is the three-dimensional view of the same film. Here, the morphological characteristics of VPtCl$_6$ film observed were consistent with their SEM images. The size and shape of the particles were the same as in SEM. Generally the roughness of the surface will increase the electrocatalytic activity of the film surface.[39] Here, the roughness average (sa) for the whole surface area (10,000 × 10,000 nm) was 21.9 nm. Further, the remaining parameters like skewness, kurtosis, etc., will clearly explain the surface nature of the film. By using a combination of the skewness and kurtosis values, it is possible to identify the surfaces that have a relatively flat top, but contain deep valleys.

The skewness (ssk) measures the symmetry of the variation of a surface about its mean plane. The positive value (0.986) of the ssk of the film shows that the surface is comprised of a disproportionate number of peaks, indicating the uneven deposition of platinum and vanadium. Kurtosis (sku) is a measure of the unevenness or sharpness of the surface. A surface that is centrally distributed has an sku value greater than 3. Here, for this film the sku value is 3.85. The other functional parameters like the core roughness depth (Sk), the Svk (reduced valley depth) was 58.1 and 18.7 nm for the VPtCl$_6$ film, respectively. Finally, from the topographical three-dimensional image and cross-sectional profile analysis (Fig. 8E), we construe the surface nature of the VPtCl$_6$ film on the electrode surface.

Electrocatalytic reduction of NAD$^+$.— The electrocatalytic reduction of NAD$^+$ by VPtCl$_6$ film-modified GCE was performed in an oxygen-free 0.1 M aqueous KCl solution (pH 3.0) containing 1 × 10^{-3} M V^{2+} (Fig. 9). The electrocatalytic reduction peaks of NAD$^+$ at VPtCl$_6$-modified GCE could be found at −0.51 V (vs Ag/AgCl). The reduction peak current for NAD$^+$ increased linearly with the concentration range of 1 × 10^{-4} to 5 × 10^{-4} M, respectively (curves a–d). Further, the curve a′ shows that the bare GCE fails to produce the reduction peak for NAD$^+$. The acquired result confirms the electrocatalytic activity of VPtCl$_6$ film for the electrocatalytic reduction of NAD$^+$.[37,40,41] Furthermore, the obtained result is comparable with previous results reported for the electroanalytical determination of NAD$^+$ at different types of film-modified electrodes (Table II). The expected reaction mechanism for NAD$^+$ reduction using the VPtCl$_6$ film-modified electrode is described below[40,42]

$$NAD^+ + e^- \rightarrow NAD \qquad [10]$$

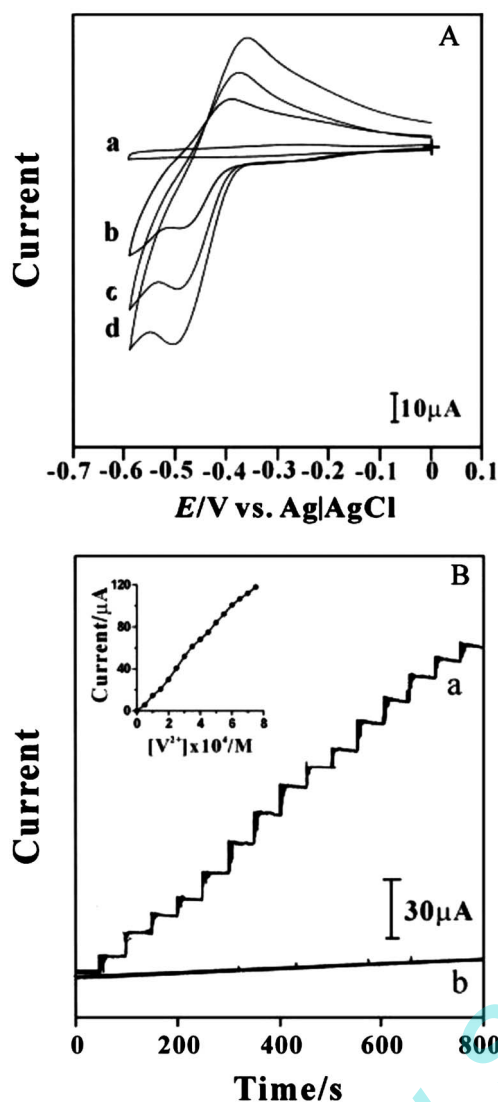The proposed scheme for NAD$^+$ reduction is shown in Scheme 2.

Figure 6. (A) Cyclic voltammogram of a VPtCl$_6$ film adhered to a GCE in a 0.1 M aqueous KCl solution at pH 3.0 with various concentrations of V^{2+}: (a) 0, (b) 1 × 10^{-3}, (c) 2 × 10^{-3}, (d) 3 × 10^{-3} M. Scan rate = 0.1 V s^{-1}. (B) Amperometric responses of 15 sequential additions of V^{2+} (each 5 × 10^{-5} M) at GCE modified with a VPtCl$_6$ film, (b) bare GCE. Rotation rate = 1200 rpm. E_{appl} = −0.7 V (vs Ag/AgCl). The inset shows a plot of cathodic current vs [V^{2+}].

state within a short time. The reduction current of the VPtCl$_6$ film with the addition of V^{2+} on the bare GC disk electrode was carried out in the above-mentioned conditions and compared with the above results. Here, the reduction current with various concentrations of V^{2+} using a bare disk GCE showed a very small current (Fig. 6B, part b) when compared to that using the VPtCl$_6$ film/GC-modified disk electrode (Fig. 6B, part a) carried out in the above-mentioned conditions. Thus, the results ascertain that the VPtCl$_6$ film formation was obvious in the presence of V^{2+} in the acidic (pH 3.0) aqueous solution.

SEM and AFM characterization.— Figure 7 shows a typical SEM micrograph obtained for the VPtCl$_6$ film electrodeposited onto the ITO. A general inspection of the SEM result demonstrates that the film contains both vanadium and platinum particles as a layer. Here, the Pt has exhibited an unpredictable shape spread over with small-size vanadium particles. From the SEM results, the surface nature of the VPtCl$_6$ film was authenticated. Further, the same film
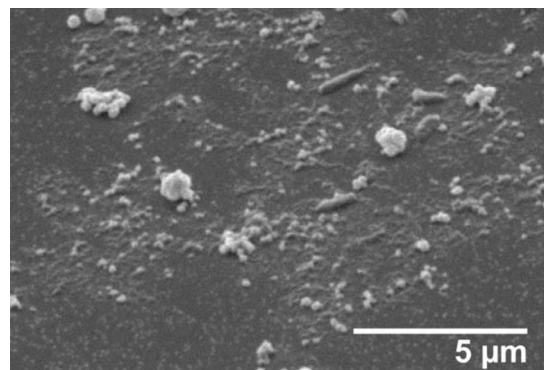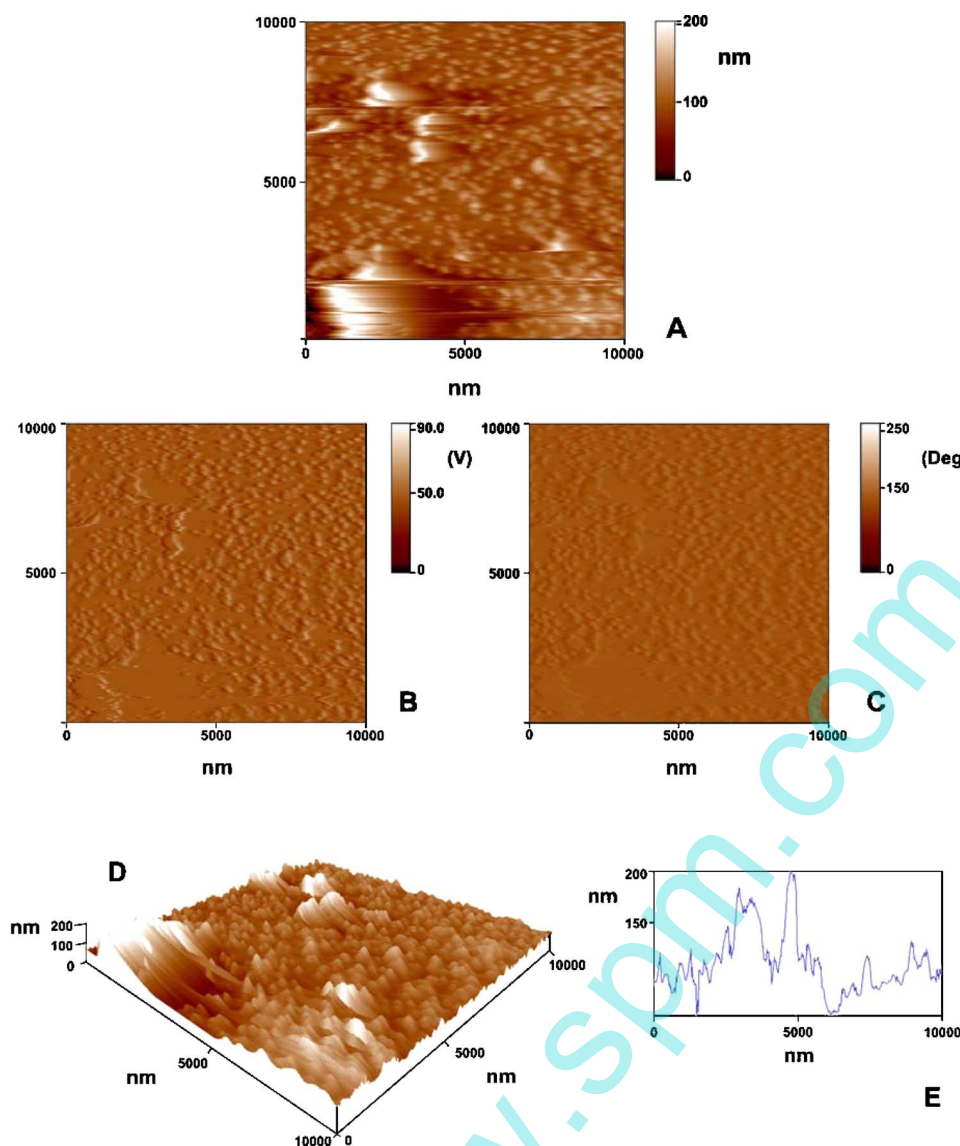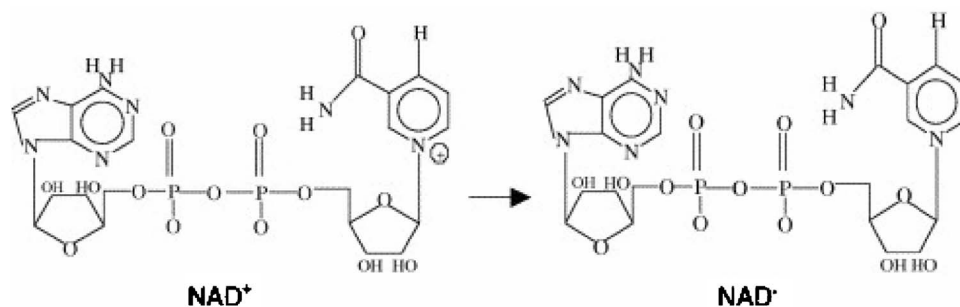
Figure 8. (Color online) (A) Topographic, (B) amplitude, (C) phase view of VPtCl$_6$ film deposited on ITO. (D), (E) Three-dimensional view and cross-sectional graph of the VPtCl$_6$ film.

Electrocatalytic reduction of sulfur oxoanions.— The VPtCl$_6$ film-modified GCE could be used to study the electrocatalytic reduction reactions of sulfur oxoanions like S$_4$O$_6^{2-}$, S$_2$O$_8^{2-}$, and SO$_5^{2-}$ (Fig. 10A-10C). The electrocatalytic reduction of these sulfur oxoanions in nitrogen saturated aqueous solution exhibited an Ep_{cat} close to the Ep_c of VPtCl$_6$ redox couple (Fig. 10A-10C) and the reduction occurred at around 0.5 V. For the S$_4$O$_6^{2-}$ reduction, the cathodic peak current increased significantly according to the increasing concentration of S$_4$O$_6^{2-}$ in pH 3.0 KCl aqueous solution. Here, the cathodic peak current increased concomitantly with the decrease of the anodic peak current. The reduction current of S$_4$O$_6^{2-}$ developed directly from the redox couple of VPtCl$_6$ film at a peak potential between 0.0 and −0.50 V. A similar type of results was obtained for the various concentrations of S$_2$O$_8^{2-}$ and SO$_5^{2-}$ oxoanions (Fig. 10B and 10C) at VPtCl$_6$ film-modified GCE. Furthermore, the Ip_{cat} value increased with increasing concentration of S$_2$O$_8^{2-}$ and SO$_5^{2-}$. In the case of the S$_2$O$_8^{2-}$ reduction process at this modified electrode, SO$_4^{2-}$ and SO$_4^-$ are the expected reduced products of S$_2$O$_8^{2-}$.[43-45] The comparison of reduction potentials for sulfur oxoan-

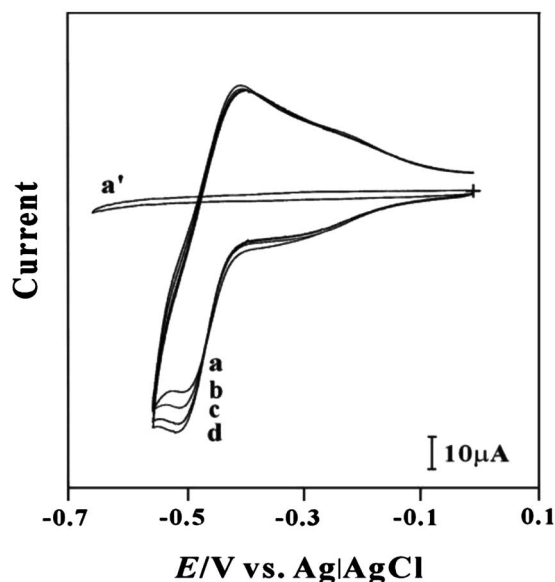**Scheme 2.** The proposed scheme for NAD$^+$ reduction.

Figure 9. Cyclic voltammogram of a VPtCl$_6$ film adhered to a GCE for 1 × 10^{-3} M V^{2+} in a 0.1 M aqueous KCl solution at pH 3.0 with various concentrations of NAD$^+$: (A) 0.0, (B) 1 × 10^{-4}, (C) 3 × 10^{-4}, (D) 5 × 10^{-4} M. Scan rate = 0.1 V s^{-1}. (a′) bare GCE and [NAD$^+$] = 5 × 10^{-4} M.

ions with earlier reports is listed in Table III. These results ascertain the practical application of vanadium hexachloroplatinate film-modified electrodes as electrochemical sensors to determine various sulfur oxoanions. To evaluate the lifetime of VPtCl$_6$ film-modified GCE, it was stored in an aqueous solution at room temperature and the analytical determinations for NAD$^+$ and sulfur oxoanions were examined for 1 week. The results showed that the analytical values determined by VPtCl$_6$-modified GCE for the detection of NAD$^+$ and sulfur oxoanions were constant for 4 days.

Conclusions

In conclusion, the electrochemically active and stable VPtCl$_6$ film was directly synthesized from the mixing of V^{2+} and PtCl$_6^{2-}$ ions in aqueous KCl pH 3.0 solutions on various electrodes using repetitive cyclic voltammetry. An EQCM, cyclic voltammetry, amperometry, and UV-visible absorption spectroscopy were used to study the interaction of V^{2+} and PtCl$_6^{2-}$ ions and the in situ growth of these two types of films. The surface morphology of the film was ascertained by means of SEM and AFM. The experimental results indicate that the redox process of the vanadium hexachloroplatinate (VPtCl$_6$) film is confined to the surface, confirming its immobilized state. The deposition of a VPtCl$_6$ film occurred when Pt^{IV}Cl$_6^{2-}$ was electrochemically reduced to Pt^{II}Cl$_6^{4-}$ and V^{3+} to V^{2+}. The reversibility of the vanadium (II/III) hexachloroplatinate film during cycling and with changing frequency was found to be good, and the V^{2+} ion exchange obviously occurred in the redox couples. Furthermore, the VPtCl$_6$ film electrocatalytically reduced NAD$^+$, SO$_5^{2-}$, S$_2$O$_8^{2-}$, and S$_4$O$_6^{2-}$ through the redox couple of the vanadium (II/III)
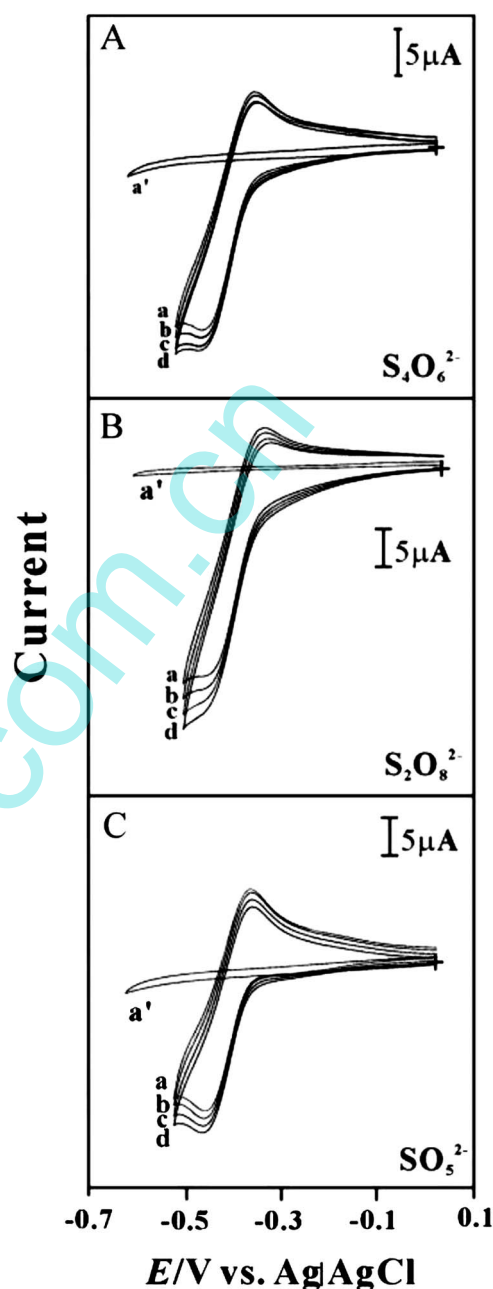

Figure 10. Cyclic voltammogram of a VPtCl$_6$ film adhered to a GCE for 1 × 10^{-3} M V^{2+} in a 0.1 M aqueous KCl solution at pH 3.0 with various concentrations of: (A) [S$_4$O$_6^{2-}$] = (a) 0.0, (b) 1.5 × 10^{-4}, (c) 2.5 × 10^{-4}, (d) 3 × 10^{-4} M. (a′) bare GCE and [S$_4$O$_6^{2-}$] = 3 × 10^{-4} M, (B) [S$_2$O$_8^{2-}$] = (a) 0.0, (b) 2 × 10^{-4}, (c) 3 × 10^{-4}, (d) 4 × 10^{-4} M. (a′) Bare GCE and [S$_2$O$_8^{2-}$] = 4 × 10^{-4} M, (C) [SO$_5^{2-}$] = (a) 0.0, (b) 1.5 × 10^{-4}, (c) 2.5 × 10^{-4}, (d) 3 × 10^{-4} M. (a′) bare GCE and [SO$_5^{2-}$] = 3 × 10^{-4} M. Scan rate = 0.1 V s^{-1}.

Table II. Comparison of VPtCl$_6$/GCE with other methods for NAD$^+$ reduction.

S. No.	Type of film-modified GCE	Linear range (10^{-5} M)	NAD$^+$ reduction potential (V)	pH	Ref.
1.	Cerium hexachloroplatinate	20–60	−0.55	3.0	37
2.	Iron hexachloroplatinate	200–600	−0.51	3.0	40
3.	Tin hexachloroplatinate	10–30	−0.50	3.0	41
4.	Vanadium hexachloroplatinate	10–50	−0.52	3.0	This work

Table III. Comparison of sulfur oxoanion reduction peak potentials at VPtCl$_6$/GCE with other methods.

S. No.	Type of film-modified GCE	Sulfur oxoanion's electrocatalytic reduction potentials (V)			pH	Ref.
		$S_4O_6^{2-}$	$S_2O_8^{2-}$	SO_5^{2-}		
1	Iron tetrakis (N-methyl-2-pyridyl)porphyrin	−0.75	–	–	9.0	14
2.	Iron tetrakis(4-sulfonatophenyl) porphyrin	−1.25	–	–	5.5	15
3.	Ruthenium oxide/hexacyanoruthenate	–	−0.1	−0.1	5.0	20
4.	Tin hexachloroplatinate	−0.58	−0.5	−0.6	3.0	41
5.	Cerium hexachloroplatinate	−0.65	–	−0.55	3.0	37
6.	Osmium oxide/hexacyanoruthenate	–	–	−0.15	4.0	44
7.	Poly(acriflavine)	–	+0.15	+0.16	3.5	45
8.	Vanadium hexachloroplatinate	−0.50	−0.48	−0.47	3.0	This work

hexachloroplatinate species. The electrochemical reaction of V^{2+} and VPtCl$_6$ film was also investigated using an amperometric experiment.

References

1. Y.-T. Long and H.-Y. Chen, *J. Electroanal. Chem.*, **440**, 239 (1997).
2. M. Beley and J.-P. Collin, *J. Mol. Catal.*, **79**, 133 (1993).
3. A. A. Karyakin, O. A. Bobrova, and E. E. Karyakina, *J. Electroanal. Chem.*, **399**, 179 (1995).
4. X. Chen, J. M. Fenton, R. J. Fisher, and R. A. Peattie, *J. Electrochem. Soc.*, **151**, E56 (2004).
5. S. Kim, S.-E. Yun, and C. Kang, *Electrochem. Commun.*, **1**, 151 (1999).
6. S. Kim, S.-E. Yun, and C. Kang, *J. Electroanal. Chem.*, **465**, 153 (1999).
7. M. L. Coleman, D. B. Hedrick, D. R. Lovely, D. C. White, and K. Pye, *Nature (London)*, **361**, 436 (1993).
8. B. Ginzburg, I. Chlifa, J. Gun, I. Dor, O. Hadas, and O. Lev, *Environ. Sci. Technol.*, **32**, 2130 (1998).
9. B. Ginzburg, I. Dor, I. Chalifa, O. Hadas, and O. Lev, *Environ. Sci. Technol.*, **33**, 571 (1999).
10. J. Z. Zhang and F. J. Miller, *Anal. Chim. Acta*, **284**, 497 (1994).
11. P. L. Miller, D. Vasudevan, P. M. Gschwend, and A. L. Roberts, *Environ. Sci. Technol.*, **32**, 1269 (1998).
12. K. Sonne and P. K. Dasgupta, *Anal. Chem.*, **63**, 427 (1991).
13. J. Radford-Knoery and G. A. Cutter, *Anal. Chem.*, **65**, 976 (1993).
14. S.-M. Chen, *Inorg. Chim. Acta*, **244**, 155 (1996).
15. S.-M. Chen, *J. Electroanal. Chem.*, **407**, 123 (1996).
16. G. Shi, M. Luo, J. Xue, Y. Xian, L. Jin, and J. Y. Jin, *Talanta*, **55**, 241 (2001).
17. H. Li, H. Tu, Q. Cai, Y. Xian, and L. Jin, *Analyst*, **126**, 699 (2001).
18. D. Ravi Shankaran and S.S. Narayanan, *Sens. Actuators, B*, **55**, 191 (1999).
19. S. M. Chen, *Electrochim. Acta*, **43**, 3359 (1998).
20. S. M. Chen and S. H. Hsueh, *J. Electroanal. Chem.*, **566**, 291 (2004).
21. M. F. de Oliveira, R. J. Mortimer, and N. R. Stradiotto, *Microchem. J.*, **64**, 155 (2000).
22. G. Oriji, Y. Katayama, and T. Miura, *J. Power Sources*, **139**, 321 (2005).
23. S. Zhong and M. Skyllas-Kazacos, *J. Power Sources*, **39**, 1 (1992).
24. C. Fabjan, J. Garche, B. Harrer, L. Jorissen, C. Kolbeck, F. Philippi, G. Tomazic, and F. Wagner, *Electrochim. Acta*, **47**, 825 (2001).
25. L. F. Schneemeyer, S. E. Spengler, and D. W. Murphy, *Inorg. Chem.*, **24**, 3044 (1985).
26. K. N. Thomsen and R. P. Baldwin, *Anal. Chem.*, **61**, 2594 (1989).
27. Y. Tani, H. Eun, and Y. Umezawa, *Electrochim. Acta*, **43**, 3431 (1998).
28. M. Zadronecki, I. A. Linek, J. Stroka, P. K. Wrona, and Z. Galus, *J. Electrochem. Soc.*, **148**, E348 (2001).
29. A. R. Coon, L. J. Amos, A. B. Bocarsly, and P. A. Fitzgerald-Bocarsly, *Anal. Chem.*, **70**, 3137 (1998).
30. J. Pei and X.-Y. Li, *Electrochim. Acta*, **45**, 1581 (2000).
31. S.-M. Chen and J.-L. Lin, *J. Electroanal. Chem.*, **567**, 233 (2004).
32. A. J. Bard and L. R. Faulkner, *Electrochemical Method Fundamentals and Applications*, Wiley and Sons, New York (1980).
33. A. P. Brown and F. C. Anson, *Anal. Chem.*, **49**, 1589 (1977).
34. G. Sauerbrey, *Z. Phys.*, **155**, 206 (1959).
35. S. Bruckenstein and M. Shay, *Electrochim. Acta*, **30**, 1295 (1985).
36. Z. Tang, D. Geng, and G. Lu, *J. Colloid Interface Sci.*, **287**, 159 (2005).
37. S.-M. Chen and K.-H. Lin, *J. Electroanal. Chem.*, **586**, 145 (2006).
38. J. Pei and X.-Y. Li, *J. Electroanal. Chem.*, **441**, 245 (1998).
39. P. Ramesh, G. S. Suresh, and S. Sampath, *J. Electroanal. Chem.*, **561**, 173 (2004).
40. S.-M. Chen and J.-L. Lin, *J. Electroanal. Chem.*, **583**, 248 (2005).
41. S.-M. Chen and J.-L. Lin, *J. Electroanal. Chem.*, **571**, 223 (2004).
42. S.-M. Chen and K.-H. Lin, *J. Electroanal. Chem.*, **523**, 93 (2002).
43. G. Xu and S. Dong, *Electroanalysis*, **12**, 583 (2000).
44. S.-M. Chen, C.-J. Liao, and V. S. Vasantha, *J. Electroanal. Chem.*, **589**, 15 (2006).
45. S.-M. Chen, M.-I. Liu, and S. A. Kumar, *Electroanalysis*, **19**, 999 (2007).